ELSEVIER

Accurate computations of the laminar flow past a square cylinder based on two different methods: lattice-Boltzmann and finite-volume

M. Breuer [*], J. Bernsdorf [1], T. Zeiser, F. Durst

Lehrstuhl für Strömungsmechanik, Universität Erlangen–Nürnberg, Cauerstr. 4, D-91058 Erlangen, Germany

Abstract

The confined flow around a cylinder with square cross-section mounted inside a plane channel (blockage ratio $B = 1/8$) was investigated in detail by two entirely different numerical techniques, namely a lattice-Boltzmann automata (LBA) and a finite-volume method (FVM). In order to restrict the approach to 2D computations, the largest Reynolds number chosen was $Re = 300$ based on the maximum inflow velocity and the chord length of the square cylinder. The LBA was built up on the D2Q9 model and the single relaxation time method called the lattice-BGK method. The finite-volume code was based on an incompressible Navier–Stokes solver for arbitrary non-orthogonal, body-fitted grids. Both numerical methods are of second-order accuracy in space and time. Accurate computations were carried out on grids with different resolutions. The results of both methods were evaluated and compared in detail. Both velocity profiles and integral parameters such as drag coefficient, recirculation length and Strouhal number were investigated. Excellent agreement between the LBA and FVM computations was found. © 2000 Elsevier Science Inc. All rights reserved.

Keywords: Square cylinder flow; Lattice-Boltzmann automata; Finite-volume method; Von Kármán vortex street; Strouhal number; Drag and lift coefficient; Recirculation length

1. Introduction

The flow past bluff bodies, especially cylinders, have been an attraction in all kinds of fluid mechanical investigations for a long time. Most of these studies were concerned with the circular cylinder case under free flow conditions. Excellent reviews on this topic were written by Williamson (1996) and Zdravkovich (1997). In contrast to the overwhelming number of publications on the flow past circular cylinders, the square counterpart has not been investigated to the same extent, although it plays a dominant role in many technical applications such as building aerodynamics; for details, see, e.g., Franke (1991), Franke et al. (1990), Klekar and Patankar (1992), Davis and Moore (1982), Davis et al. (1984), Okajima (1982, 1990), Mukhopadhyay et al. (1992) and Suzuki et al. (1993). Owing to fixed separation points for sharp-edged bodies, it is generally accepted that aerodynamic coefficients are less dependent on the Reynolds number than for circular structures.

Depending on the Reynolds number, different flow regimes can be distinguished for a square cylinder (Franke, 1991). At very small Reynolds numbers ($Re < 1$), viscous forces dominate the flow. For this creeping flow, no separation takes place at the surface of the cylinder. With increasing Re, the flow separates first at the trailing edges of the cylinder and a closed steady recirculation region consisting of two symmetric vortices is observed behind the body. The size of the recirculation region increases with increase in Re. When a critical Reynolds number Re_{crit} is exceeded, the well-known von Kármán vortex street with periodic vortex shedding from the cylinder can be detected in the wake. Different values of Re_{crit} exist in the literature. Based on experimental investigations, Okajima (1982) found periodic vortex motion at $Re \approx 70$ leading to an upper limit of $Re_{crit} \leqslant 70$. A smaller value ($Re_{crit} = 54$) was determined by Klekar and Patankar (1992) based on a stability analysis of the flow. When the Reynolds number is further increased, the flow separates at the leading edges of the cylinder. The onset of this phenomenon is not clearly defined in the literature; only a wide range of $Re = 100$ to 150 is given (Okajima, 1982; Franke, 1991). In this Reynolds number range, the flow past square cylinders can still be considered as 2D. In contrast to the circular cylinder flow for which Williamson (1996) provides a Reynolds number limit of $Re \approx 180$ for the onset of 3D structures in the wake, no such clear statement can be found for the square counterpart. A rough hint is given by Franke (1991) with $Re \leqslant 300$. Therefore, this Reynolds number was chosen as the upper limit of the present 2D laminar simulations. Beyond this limit 3D structures have

[*] Corresponding author. Tel.: +49-9131-8529501; fax: +49-9131-8529503.

E-mail address: breuer@lstm.uni-erlangen.de (M. Breuer).

[1] Present address: C & C Research Laboratories, NEC Europe Ltd., Rathausallee 10, D-53757 Sankt Augustin, Germany.

to be expected and subsequently transition to turbulence takes place in the free shear layers.

Only a few studies have dealt with the influence of confining walls on the flow phenomena around square cylinders (see, e.g., Davis and Moore, 1982; Li and Humphrey, 1995). In comparison with the free flow case, two new parameters have to be taken into account, the inflow profile and the blockage ratio. As shown by Davis et al. (1984), the vortex shedding frequency depends strongly on the inflow profile. In the experimental investigations by Shair et al. (1963) and Davis et al. (1984), non-negligible deviations between the velocity profiles far upstream of the cylinder and the parabolic distribution expected for fully developed laminar channel flow were observed. Therefore, this aspect has to be kept in mind for comparison between experimental and numerical investigations which typically apply the theoretical velocity profile as inflow conditions. The second parameter which plays a dominant role in the confined cylinder flow is the blockage ratio of the channel, defined as $B = D/H$, where D is the diameter of the cylinder and H is the channel height. It is generally accepted that for a fixed Reynolds number, an increasing blockage ratio leads to an increase in the Strouhal number. This holds true for both circular and square cylinders, although the movement of the separation points cannot be responsible for this phenomenon for a sharp-edged body as assumed for a round geometry.

Davis et al. (1984) investigated the confined flow past square cylinders for a wide range of Re and two different blockage ratios ($B = 1/6$ and $1/4$), experimentally and numerically. Depending on the blockage ratio, a maximum Strouhal number was observed at $Re = Re_{max} = 200$ to 350. [2] For higher Re the Strouhal number decreases again and reaches an almost constant level. As mentioned above, non-parabolic velocity profiles were measured upstream of the cylinder. Because most numerical predictions were based on these measured inflow profiles, a direct comparison with the present study is possible only for the additional cases in which a parabolic profile was assumed. These computations were based on a finite-volume code and non-equidistant coarse grids of 76×42 and 76×52 grid points.

Two-dimensional numerical simulations were also carried out by Mukhopadhyay et al. (1992) for the Re range 90–1200, two blockage ratios ($B = 1/8$ and $1/4$) and a parabolic inflow profile. With respect to the Reynolds number of the corresponding channel flow, the upper limit of Re in this investigation seems to be highly questionable because a turbulent flow in the channel has to be expected under these conditions. For the simulations two different equidistant grids with 200×34 and 396×66 grid points were used. Because no clustering of grid points in the vicinity of the cylinder was applied, each surface was resolved by only four or eight control volumes, respectively. As will be shown below, this resolution is definitely much too coarse to provide reliable results.

Suzuki et al. (1993) performed simulations ($56.3 \leqslant Re \leqslant 225$, $B = 1/20–1/5$) on a non-equidistant grid with 207×54 grid points, claiming to have achieved grid independence. However, based on the present study, it is questionable that this is possible with the resolution used, especially for the higher Reynolds number cases in which separation starts at the leading edge of the cylinder. For a blockage ratio $B = 1/5$, Suzuki et al. (1993) computed Strouhal numbers over a wide Re range and found a maximum at $Re = Re_{max} = 150$.

A comparison of the different data mentioned above shows a large scatter of the results already for integral parameters

such as the Strouhal number (see, e.g., Fig. 9). There is evidently a lack of reliable experimental and numerical data for this flow case. The objective of the present study was to yield a contribution to close this gap. In order to provide trustworthy results, two totally different numerical methods (lattice-Boltzmann automata (LBA) and finite-volume method (FVM)) were applied and special attention was paid to the analysis of the accuracy of the solutions in terms of grid independence. For a fixed blockage ratio $B = 1/8$, the laminar 2D flow field was computed in the Reynolds number range $0.5 \leqslant Re \leqslant 300$. The results were evaluated in detail based on velocity fields and integral parameters and compared with previous numerical and experimental studies.

It should be stated clearly that the objective of this work was not to make a comparison of both numerical algorithms with respect to computational efficiency in terms of CPU time and memory requirements. This was already the topic of a previous work (Bernsdorf et al., 1999), which demonstrated that the FVM approach is more efficient for simple geometries whereas the LBA is advantageous for highly complex geometries such as those occurring in porous media (e.g. sedimentary layers). Therefore, besides the physics of the flow past a square cylinder, the paper focuses on the comparison of the accuracy of both methods. Similar investigations have been carried out by Eggels and Somers (1995) for a non-isothermal free convective flow in a square cavity and by Eggels (1996) for the direct numerical simulation of fully developed turbulent channel flow with heat transfer.

2. Description of numerical methods

In the following sections a brief introduction to the two different numerical methods is given. For a more detailed description, we refer to the literature cited.

2.1. Lattice-Boltzmann automata (LBA)

An alternative approach to the well-known finite-volume, finite-difference and finite-element techniques for solving the Navier–Stokes equations are the new lattice-gas/Boltzmann methods (Frisch et al., 1987), which treat the fluid on a statistical level, simulating the movement and interaction of single particles or ensemble-averaged particle density distributions by solving a velocity discrete Boltzmann-type equation.

The lattice-Boltzmann method has been shown to be a very efficient tool for flow simulation in highly complex geometries discretized by up to several million grid points (Bernsdorf and Schäfer, 1997; Bernsdorf et al., 1998, 1999; Zeiser, 1998). All numerical simulations presented in this paper were performed with an implementation (BEST) of the lattice-Boltzmann method proposed by Qian et al. (1992), which will be briefly described here.

For simplicity, an equidistant orthogonal lattice is chosen for common LBA computations. This could be done without a significant loss of memory and performance, since the LBA requires much less memory and CPU time than conventional FVM. On every lattice node $\vec{r}_*$, a set of i real numbers, the particle density distributions N_i, is stored. The updating of the lattice consists of basically two steps: a streaming process, where the particle densities are shifted in discrete time steps t_* through the lattice along the connection lines in direction $\vec{c}_i$ to their next neighboring nodes $\vec{r}_* + \vec{c}_i$, and a relaxation step, where locally a new particle distribution is computed by evaluating an equivalent to the Boltzmann collision integrals (Δ_i^{Boltz}). For every time step, all quantities appearing in the Navier–Stokes equations (velocity, density, pressure gradient and viscosity) can locally be computed in terms of simple

---

[2] The Reynolds number $Re = Re_{max}$ is based on the maximum velocity of the inflow profile.

functions of this density distribution and (for the viscosity) of the relaxation parameter ω.

For the present computations, a 2D nine-speed (D2Q9) lattice-Boltzmann automata with single time Bhatnagar–Gross–Krook (Bhatnagar et al. (1954)) relaxation collision operator Δ_i^{Boltz} proposed by Qian et al. (1992) is used

$$N_i(t_* + 1, \vec{r}_* + \vec{c}_i) = N_i(t_*, \vec{r}_*) + \Delta_i^{\text{Boltz}}, \tag{1}$$

$$\Delta_i^{\text{Boltz}} = \omega(N_i^{\text{eq}} - N_i) \tag{2}$$

with a local equilibrium distribution function N_i^{eq}

$$N_i^{\text{eq}} = t_p \varrho \left\{ 1 + \frac{c_{i\alpha} u_\alpha}{c_s^2} + \frac{u_\alpha u_\beta}{2 c_s^2} \left(\frac{c_{i\alpha} c_{i\beta}}{c_s^2} - \delta_{\alpha\beta} \right) \right\}. \tag{3}$$

This local equilibrium distribution function N_i^{eq} has to be computed every time step for every node from the components of the local flow velocities u_α and u_β, the fluid density ϱ, a lattice geometry weighting factor t_p and the speed of sound c_s, which we chose to recover the incompressible time-dependent Navier–Stokes equations (Qian et al., 1992)

$$\partial_t \varrho + \partial_\alpha (\varrho u_\alpha) = 0, \tag{4}$$

$$\partial_t (\varrho u_\alpha) + \partial_\beta (\varrho u_\alpha u_\beta) = -\partial_\alpha p + \mu \partial_\beta (\partial_\beta u_\alpha + \partial_\alpha u_\beta). \tag{5}$$

If the problem of proper wall boundary conditions is excepted (see discussion below), the present LBA method is of second-order accuracy in space and time (Qian et al., 1992). BEST is highly optimized for vector-parallel machines such as the NEC SX-4, the Fujitsu VPP 700 or the CRAY T90. A sustained performance of 7–8.5 million lattice site updates per second is achieved on one processor of the above-mentioned machines.

2.2. Finite-volume method (FVM)

The applied code LESOCC is based on a 3D FVM for arbitrary non-orthogonal and non-staggered grids. It was originally developed for simulating incompressible turbulent flows of practical relevance by the large eddy simulation (LES) technique (Breuer and Rodi, 1994, 1996; Breuer et al., 1996; Breuer and Pourquié, 1996; Breuer, 1998a,b, 1999). Owing to the high demands of LES with respect to spatial and temporal accuracy, the method is also well suited for the accurate computation of time-dependent laminar flows. Five different options are implemented in LESOCC for the approximation of convective fluxes. However, based on experience in previous investigations (Breuer, 1998b), only central differences of second-order accuracy are applied for both the convective and the viscous fluxes. Time advancement is performed by a predictor–corrector scheme. A low-storage multi-stage Runge–Kutta method (three sub-steps, second-order accurate in time) is applied for integrating the momentum equations in the predictor step. Within the corrector step, the Poisson equation for the pressure correction (SIMPLE) is solved implicitly by an incomplete LU decomposition method. Explicit time marching works well for LES with small time steps necessary to resolve turbulence motion in time. For time accurate predictions of laminar flows, explicit time marching is also the proper choice.

On non-staggered grids such as used in the present investigation, a special interpolation technique for the cell face velocities is necessary to avoid the decoupling of pressure and velocity components leading to non-physical oscillations. These cell face velocities are needed to determine the mass fluxes at the cell faces. The momentum interpolation of Rhie and Chow (1983) provides a proper coupling procedure. The influence of this approach on the solution was investigated in detail by Miller and Schmidt (1988) and Kobayashi and

Pereira (1991). They found that the momentum interpolation on non-staggered grids is nearly equivalent to the SIMPLE algorithm on staggered grids concerning formal error analysis and the attained accuracy of the calculations.

Of course, all models necessary to approximate the non-resolvable subgrid scales in LES are turned off for the laminar simulations. Recently, LESOCC was extended by a multi-block structure, strongly improving the possibility of resolving complex geometries. Furthermore, the multi-block implementation was also the basis for parallelization by domain decomposition and message passing (MPI). LESOCC is highly vectorized (vectorization rate $> 99.8\%$), allowing one to perform efficient computations on vector-parallel machines. Typical sustained performances are ~ 4.0 Gflops on four processors of a NEC SX-4 machine and ~ 3.7 Gflops on a Fujitsu VPP 300/700.

3. Details of the test case

3.1. Geometry of the computational domain and grids

The 2D laminar flow around a square cylinder with diameter D mounted centered inside a plane channel (height H) was investigated (see Fig. 1). The blockage ratio was fixed at $B = 1/8$. In order to reduce the influence of inflow and outflow boundary conditions, the length of the channel was set to $L/D = 50$. For the FVM computations an inflow length of $l = L/4$ was chosen. In the LBA simulations, the inflow length was varied between $l = L/4$ and $l = L/3$ to investigate the influence of different inflow and outflow lengths. However, only negligible deviations in the results were found.

The LBA method allows the application of simple orthogonal equidistant lattices/grids. This lattice type makes (semi-automatic) integration of arbitrary complex geometries very easy: single lattice nodes are either occupied by an elementary obstacle or they are free (marker and cell approach). The FVM is written for general body-fitted curvilinear coordinates. Owing to the specific geometry in the present study, only Cartesian grids are applied. However, in contrast to the LBA, the FVM allows the application of non-equidistant stretched grids. This has the advantage that grid points can be clustered in regions of large gradients (e.g. in the vicinity of the cylinder) and coarser grids can be used in regions of minor interest. Consequently, fewer grid points are necessary for the FVM to achieve the same accuracy as the LBA. Table 1 gives an overview of all grids used in the present study. Four different equidistant grids with up to 640,000 lattice nodes were generated for the LBA. The number of lattice nodes on each side of the square cylinder varies between 10 and 40, leading to smallest distances between lattice nodes of $0.1D$ to $0.025D$. Three different grids were used for the FVM. The first is equal to the coarsest grid for LBA. The second and third are stretched grids (geometrical series) where the grid points are highly clustered in the vicinity of the cylinder. On the finest grid each
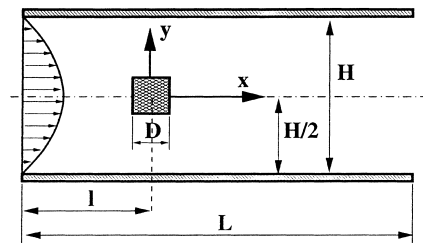

Fig. 1. Definition of the geometry and integration domain.

Table 1
Overview of all grids used

Method	Total number of CV	Grid type	Number of CV on cylinder	Smallest CV at cylinder/D	Maximum stretching factor
LBA	500×80	Equidistant	10	0.1	1
LBA	1000×160	Equidistant	20	0.05	1
LBA	1500×240	Equidistant	30	0.033	1
LBA	2000×320	Equidistant	40	0.025	1
FVM	500×80	Equidistant	10	0.1	1
FVM	400×240	Non-equidistant	80	0.01	1.03
FVM	560×340	Non-equidistant	100	0.01	1.02

face of the cylinder is discretized by 100 control volumes (CV) and the smallest CV has a chord length of 0.01D, which is 2.5 times smaller than on the finest grid for LBA.

3.2. Boundary conditions

3.2.1. Wall boundary conditions

There is a long and still ongoing discussion on the proper use of wall boundary conditions within the framework of LBA (Noble et al., 1995a,b; Ziegler, 1993; Skordos, 1993; Inamuro et al., 1995). It is often argued that the so-called 'bounce back' wall boundary conditions, which are also used in the present implementation (BEST) of the LBA scheme, are of first-order accuracy, whereas the lattice-Boltzmann equation is of second-order. However, recent investigations showed that the error produced by the bounce back boundary condition is sufficiently small if the relaxation parameter ω is close enough to 2 (Inamuro et al., 1995), allowing a precise knowledge of the wall position with zero flow velocity. Therefore, we believe that the bounce back conditions can be used without any influence on the order of the LBA scheme, if ω is chosen within a suitable range. Furthermore, the bounce back condition is the most efficient one for arbitrary complex geometries, which are most typical for the application of LBA.

In the framework of FVM for laminar flows, solid walls can be easily modeled by Stokes' no-slip wall boundary condition assuming $\vec{v} = 0$ at the wall. In contrast to the bounce back condition for LBA, there is no question about the no-slip condition for incompressible flows.

3.2.2. Inflow boundary conditions

In order to simulate a fully developed laminar channel flow upstream of the square cylinder, a parabolic velocity profile with a maximum velocity u_{max} is prescribed at the channel inlet. This velocity was chosen to be lower than 10% of the speed of sound for the LBA simulations to avoid significant compressibility effects which are known to increase with the square of the Mach number (Maier and Bernard, 1997). For the LBA the pressure at the inlet is extrapolated upstream, and the equilibrium density distribution (Eq. (3)) was computed from that pressure and the given velocity and imposed at the first lattice column. The inlet region was chosen to be long enough to ensure that a slight error which occurs when only the equilibrium distribution is taken into account has no influence on the results presented hereafter. The FVM does not require any boundary condition for the pressure.

3.2.3. Outflow boundary conditions

At the outflow boundary slightly different boundary conditions are used for LBA and FVM. However, owing to the extremely large integration domain behind the cylinder, no influence is expected for the solution in the vicinity of the

cylinder. For LBA a fixed pressure is imposed in terms of the equilibrium distribution function on the outlet. For this task, the velocity components are extrapolated downstream. For the finite-volume code a convective boundary condition given by

$$\frac{\partial u_i}{\partial t} + u_{conv} \frac{\partial u_i}{\partial x} = 0 \qquad (6)$$

is used at the outflow boundary, where u_{conv} was set equal to the maximum velocity u_{max} of the inflow profile. This condition ensures that vortices can approach and pass the outflow boundary without significant disturbances or reflections into the inner domain. In all previous computations of different test cases (Breuer and Rodi, 1994, 1996; Breuer and Pourquié, 1996; Breuer, 1998b, 1999), the convective boundary condition was found to work very well. Likewise, no difficulties were observed in the case of the square cylinder flow.

4. Results and discussion

A Reynolds number range $0.5 \leqslant Re \leqslant 300$ was investigated numerically, where Re is based on the cylinder diameter D and the maximum flow velocity u_{max} of the parabolic inflow profile. The following section starts with a description of the different flow patterns observed with increasing Re. The subsequent sections present a detailed comparison of the computed results (LBA and FVM) based on velocity profiles at several positions in the flow field. Furthermore, the computations are analyzed and compared regarding integral flow parameters such as recirculation length, Strouhal number and dimensionless force coefficients (lift and drag).

4.1. Flow pattern

Fig. 2 shows computational results (FVM) in the vicinity of the cylinder by streamlines at four different Reynolds numbers ($Re = 1, 30, 60, 200$), each characterizing a totally different flow regime. At low $Re \leqslant 1$, the creeping steady flow past the square cylinder persists without separation (Fig. 2(a)). The magnitude of viscous forces decreases with increasing Re until a certain value, at which separation of the laminar boundary layers occurs. In comparison with the circular counterpart, for which a value of $Re \approx 5$ was found (Zdravkovich, 1997), separation at the trailing edges of the sharp-edged body can be observed at lower Re. Above this limit the wake comprises a steady recirculation region of two symmetrically placed vortices on each side of the wake, as shown in Fig. 2(b) at $Re = 30$, whose length grows as Re increases. The same trend was observed for circular cylinders. Owing to the sharp corners, the separation point is fixed at the trailing edge and the flow is attached at the side walls. The steady, elongated and closed near-wake becomes unstable when $Re > Re_{crit}$ (Fig. 2(c)). The transverse oscillation starts at the end of the near-wake and initiates a
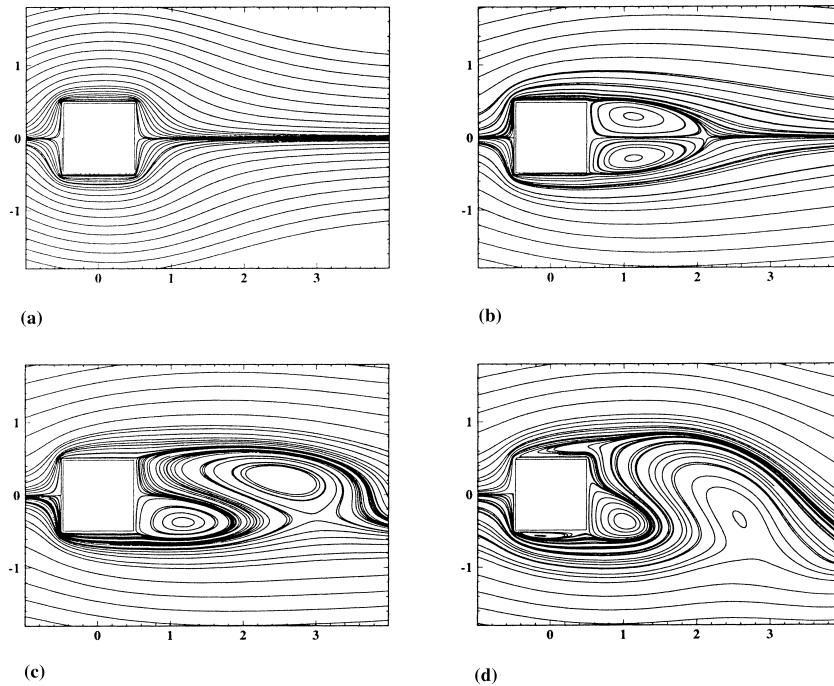
Fig. 2. Streamlines around the square cylinder for different Reynolds numbers (a) $Re = 1$; (b) $Re = 30$; (c) $Re = 60$; (d) $Re = 200$.
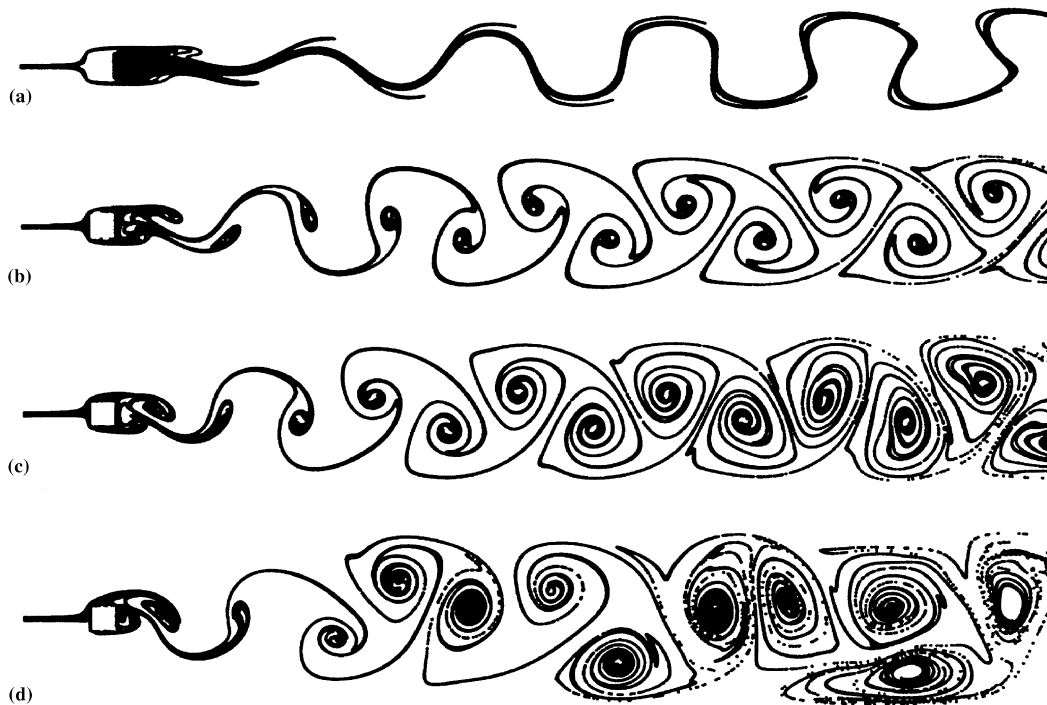

Fig. 3. Streaklines around the square cylinder for different Reynolds numbers (a) $Re = 60$; (b) $Re = 100$; (c) $Re = 200$; (d) $Re = 300$.

wave along the trail. This phenomenon is visualized by streaklines in Fig. 3(a) ($Re = 60$). Weightless particles released at different sources in front of the cylinder were integrated during the time-dependent flow computation. For the circular cylinder the onset of the wake instability was found to be a manifestation of a Hopf bifurcation (Williamson, 1996) and there is no counter-argument available to indicate that the same mechanism is responsible for the square cylinder. As

stated in Section 1, Klekar and Patankar (1992) determined a critical value of $Re_{crit} = 54$. Although this limit depends on flow parameters such as the blockage ratio, a similar value ($Re_{crit} \approx 60$) was observed in the present computations. When Re is further increased the free shear layers begin to roll up and form eddies as shown in Fig. 3(b) at $Re = 100$. This phenomenon is well known as the von Kármán vortex street. The wavelength of vortex shedding decreases with rising Re, as seen

in Fig. 3(a)–(c). Another important change in the flow structure is observed in the range $Re = 100$ to 150, where separation already starts at the leading edge of the cylinder (Fig. 2 (d), $Re = 200$). As will be seen below, this strongly influences the frequency of vortex shedding. The upper limit of this laminar 2D shedding has an enormous spread in the literature. Preliminary 3D simulations have shown that the flow computation shown in Fig. 3(d) at $Re = 300$ is slightly beyond the limit where 2D simulations can be carried out. The deviations from fully periodic structures in the far-wake are also a clear hint for this statement. Furthermore, it should be taken into account that the Reynolds number based on the channel height H and the mean velocity u_{mean} in the channel is already $Re_{channel} = 1600$ for this case. Therefore, owing to the triggering effect of the obstacle on the channel flow, transition to turbulence has to be expected leading to 3D structures in the wake.

4.2. Steady flow: $0.5 \leqslant Re < 60$

4.2.1. Recirculation length

The length of the closed near-wake (L_r) has been measured for a circular cylinder, eliminating the effect of blockage by extrapolating the measured data to $B \to \infty$. Then the empirical relationship is linear (Zdravkovich, 1997)

$$L_r/D = 0.05\,Re \quad \text{for } 4.4 < Re < 40. \tag{7}$$

Fig. 4 summarizes the computed values for the recirculation length L_r for a square cylinder inside a channel as a function of the Reynolds number. First, in Fig. 4(a) the FVM results obtained on the three different grids are compared in order to prove grid independence. On the coarsest grid the recirculation length is slightly shorter than that on the medium and fine grid. The agreement between the two non-equidistant grids is excellent over the entire Reynolds number range. No improvements can be expected by further grid refinement. Fig. 4(b) shows a comparison of the LBA and FVM results based on the finest grids used for both the methods (see Table 1). The computed values for L_r coincide extremely well, showing a linear dependence on the Reynolds number. Similarly to the relationship (7) for the circular cylinder, a curve fit of the square cylinder results ($B = 1/8$) leads to

$$L_r/D = -0.065 + 0.0554\,Re \quad \text{for } 5 < Re < 60, \tag{8}$$

which is also plotted in Fig. 4(b). As a consequence, the recirculation length of the confined square cylinder flow is slightly shorter in comparison with the circular counterpart in free stream for Reynolds numbers below $Re \approx 12$ and larger

above this value. Unfortunately, no experimental data for comparison can be found in the literature for the square cylinder.

4.2.2. Drag coefficient

One of the most important characteristic quantities of the flow around a cylinder is the drag coefficient C_d. In the region of small Reynolds numbers the drag coefficient varies strongly with Re. The contributions of the viscous and pressure forces to the total drag are of the same order of magnitude. A comparison of the computed FVM results on the three different grids is shown in Fig. 5(a) for the steady-state results in the range $0.5 \leqslant Re \leqslant 60$. On the coarsest grid the drag coefficient is slightly smaller than on the medium and fine grid, especially at the lower end of the Re range. The agreement between the results of the two non-equidistant grids is excellent over the entire Reynolds number range. As mentioned before, no improvements are expected on further grid refinement. Fig. 5(b) shows a comparison of the LBA and FVM data on the finest grid levels for $10 \leqslant Re \leqslant 60$. Deviations between the LBA and FVM results occur for small Reynolds numbers, whereas the agreement for the upper Re range considered is satisfactory. As the discrepancies are larger in the lower Re range, where the viscous forces play a dominant role for the drag, it can be concluded that an insufficient resolution of the boundary layers by the LBA method is responsible for this behavior. This also agrees with the observations based on the FVM results on the coarsest grid, which show larger discrepancies with the fine grid solutions at the lower end of the Re range.

4.3. Unsteady flow: $60 \leqslant Re \leqslant 300$

4.3.1. Velocity profiles

In order to make a detailed comparison of the LBA and FVM results, velocity profiles at different positions in the flow field were extracted for $Re = 100$. As the flow is unsteady at this Re, it was first necessary to define the moment of evaluation. In the present study this is given by the time level at which the cross-stream velocity V at an axial position of $10D$ behind the cylinder ($x = 10.5$, $y = 0$) changes its sign from minus to plus. Fig. 6 shows the velocity distribution of both velocity components along the centerline. Both LBA and FVM results were achieved on the finest grid (Table 1). The agreement between the LBA and FVM simulations is excellent in the upstream region, in the vicinity of the cylinder and also in the downstream region up to about $12D$. In the far-wake $> 12D$ small deviations occur. However, these can be
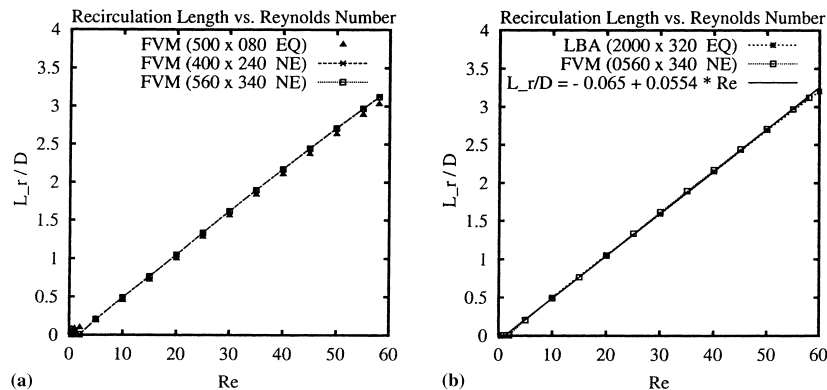

Fig. 4. Computed recirculation length L_r vs. Reynolds number. (a) Comparison of different FVM results; (b) comparison of FVM and LBA results on finest grids.
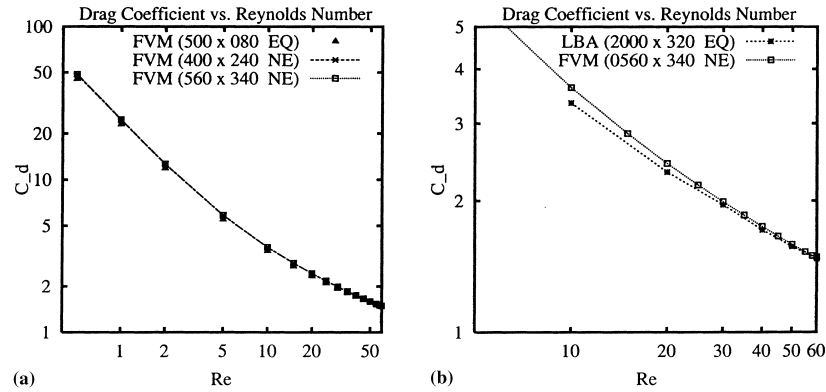
Fig. 5. Computed drag coefficient C_d vs. Reynolds number for steady flow. (a) Comparison of different FVM results; (b) comparison of FVM and LBA results on finest grids.
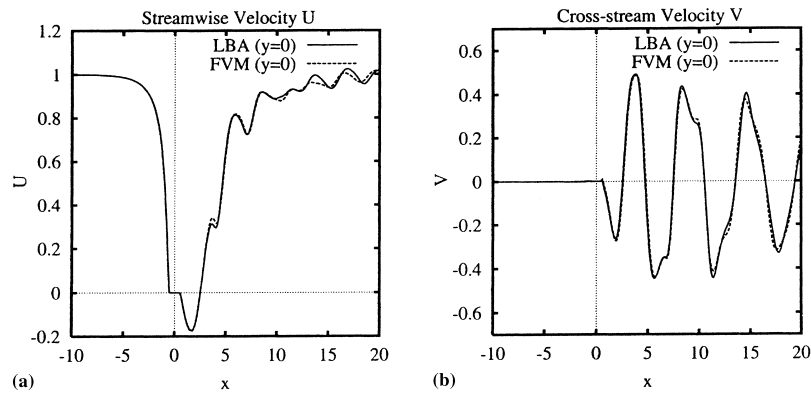

Fig. 6. Comparison of instantaneous LBA and FVM results at a certain moment (see text for explanation): (a) streamwise (U) and (b) cross-stream (V) velocities along the centerline ($y = 0$), $Re = 100$.
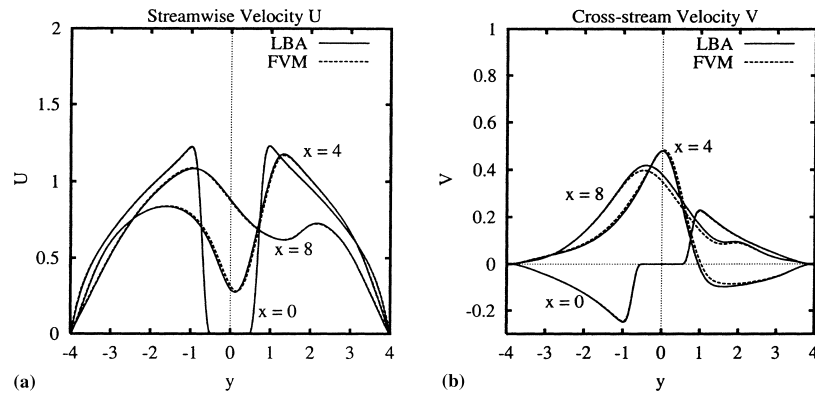

Fig. 7. Comparison of instantaneous LBA and FVM results at a certain moment (see text for explanation): (a) streamwise (U) and (b) cross-stream (V) velocities at three different positions in the flow field, center of cylinder ($x = 0$), near-wake ($x = 4$) and far-wake ($x = 8$), $Re = 100$.

explained. Owing to the stretched grids used in the FVM computations, the resolution in the vicinity of the cylinder is higher than that for the LBA simulations, whereas in the far-wake the grid is much coarser. This is a typical configuration when flows around bodies are investigated and special attention is paid to the vicinity of the structure. Owing to the present version of the LBA (equidistant grids), this strategy was not applied, leading to a higher resolution and therefore more accurate results for LBA compared with FVM.

Fig. 7 shows velocity profiles of U and V at three different axial positions, $x = 0$, 4 and 8. For the profile through the center of the cylinder ($x = 0$), no deviations are visible between the two sets of results. Further downstream small deviations occur, especially for the V component which is smaller than U and therefore more difficult to predict correctly. For the assessment of the agreement between the results of the different numerical methods, it should be taken into account that the flow is very unsteady. Therefore, the definition of the moment

of evaluation has a strong influence on the results. Owing to finite time steps (and also finite spatial resolution), the accuracy in time is in the worst case one time step size. Therefore, an exact agreement between the computational results cannot be expected.

4.3.2. Strouhal number

One important quantity taken into account in the present analysis is the Strouhal number St, computed from the cylinder diameter D, the measured frequency of the vortex shedding f and the maximum velocity u_{max} at the inflow plane

$$St = \frac{fD}{u_{max}}. \tag{9}$$

The characteristic frequency f was determined by a spectral analysis (fast Fourier transformation, FFT) of time series of the lift coefficient C_l. Fig. 8 summarizes the computational results of both methods, where the LBA data are represented by lines and the FVM results are given by symbols (partly with lines). All simulations, including those on the coarse grids, agree fairly well in the Re range $60 \leqslant Re \leqslant 133$, showing an increase in the Strouhal number with increasing Re. At the upper limit of this range an important change in the flow structure takes place, namely the movement of the separation point from the trailing edge to the leading edge of the square cylinder. As expected, the separation on the side walls is strongly influenced by the resolution in the vicinity of the
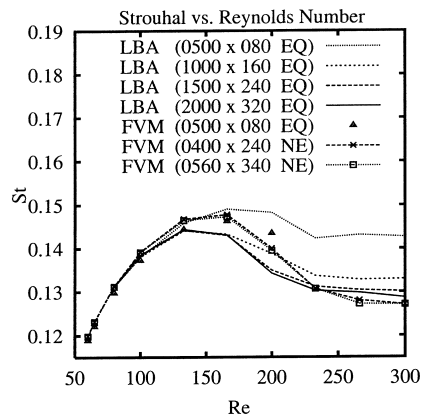
body. Therefore, the results of both methods on the coarsest grid with only 10 points on each surface do not have to be discussed seriously. At the finest resolution of the LBA, each side of the cylinder is represented by 40 nodes with a smallest distance to the wall of $0.025D$. The FVM applies 100 CV at each surface on the finest level with a 2.5 times smaller wall distance (stretched grid), resulting in a much finer resolution for the vicinity of the cylinder. Therefore, the small discrepancies between the computed Strouhal numbers of LBA and FVM at $Re > 133$ are probably due to the insufficient resolution of the recirculation regions at the side walls for LBA. However, owing to resource limitations, no further refinement was taken into account for the LBA. The Strouhal number has a maximum at about $Re = 150$ to 160 and decreases again for higher Re. With the exception of the results on the coarsest grids, the agreement between the LBA and FVM data is reasonable.

In order to demonstrate this good coincidence in comparison with data from the literature, Fig. 9 provides a collection of different numerical investigations for blockage ratios $B = 0$ to $1/4$. No experimental data are available for a parabolic inflow profile. Mukhopadhyay et al. (1992) carried out numerical simulations for the Re range $90 \leqslant Re \leqslant 1200$ with equidistant grids of up to 396×66 CV, resulting in an extremely coarse resolution of 8×8 grid points on the side walls of the cylinder. For $B = 1/8$ the Strouhal numbers increase with increase in Re without showing a maximum. In comparison with the present results included in Fig. 9, the Strouhal numbers of Mukhopadhyay et al. (1992) are much smaller. However, especially the St values for high Re are highly questionable because the flow should be turbulent inside the channel at the upper limit of the computed Re range. For $B = 1/4$ the St curve looks totally different and has a maximum at $Re \approx 200$. Suzuki et al. (1993) also carried out numerical investigations. They applied a non-equidistant grid with 207×54 CV. Three different blockage ratios ($B = 1/20, 1/10, 1/5$) were evaluated. However, only for $B = 1/5$ are enough values available to determine the St (Re) relationship plotted in Fig. 9. The curve has a maximum at $Re \approx 150$ and is in good agreement with the results of the present study, although the blockage ratio is higher. Davis et al. (1984) investigated this flow problem experimentally and numerically for $B = 1/6$ and $1/4$. However, in the experimental investigations non-parabolic inflow profiles were detected. For the numerical simulations only one St value is given for each blockage ratio in the Re range of the present work. Franke et al. (1990) computed the laminar cylinder flow under free stream conditions ($B = 0$). They found a similar
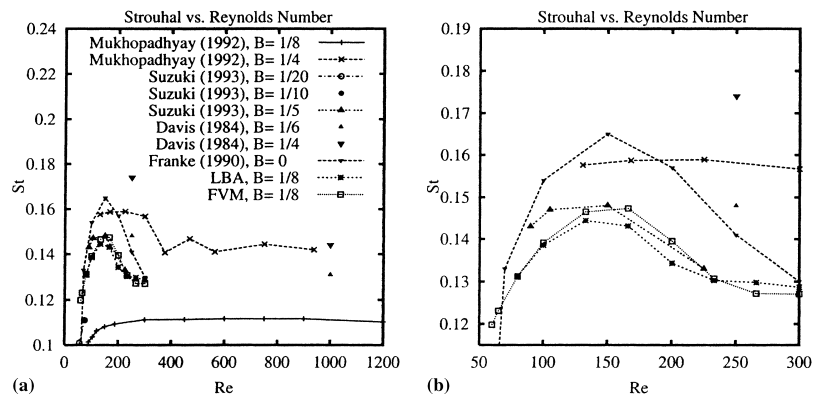

Fig. 8. Computed Strouhal numbers vs. Reynolds number for LBA and FVM on different grids.

Fig. 9. Comparison of computed Strouhal numbers (LBA and FVM) on finest grids with data from the literature. (a) Entire St (Re) range; (b) zoom of the interesting region, same legend as in (a).
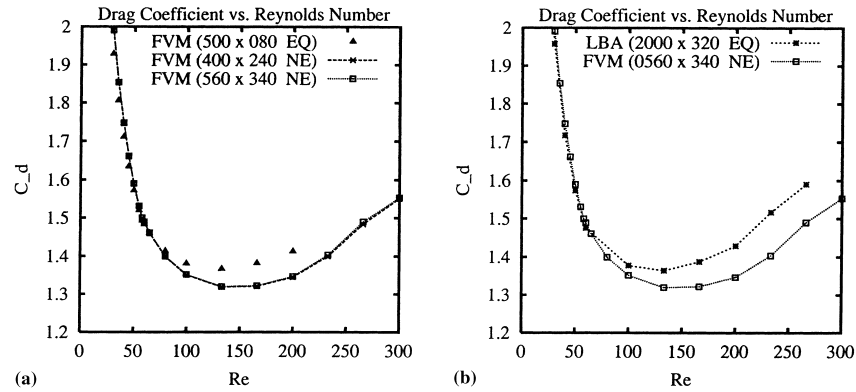
Fig. 10. Computed time-averaged drag coefficient C_d vs. Reynolds number Re for unsteady flow. (a) Comparison of different FVM results; (b) comparison of FVM and LBA results on finest grids.
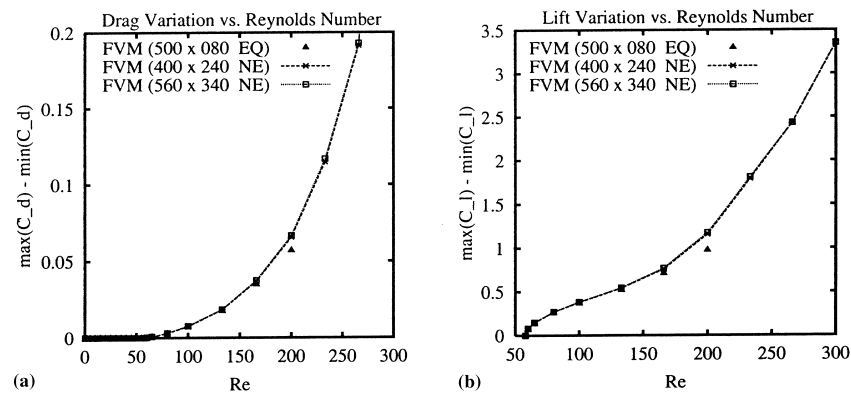

Fig. 11. Variation of force coefficient vs. Reynolds number for FVM results. (a) Drag variation, $\max(C_d) - \min(C_d)$; (b) lift variation, $\max(C_l) - \min(C_l)$.

$St(Re)$ curve to that in the present investigation with a maximum at $Re \approx 150$. However, the St values are slightly higher than the LBA and FVM results in the present study ($B = 1/8$), although it is well known that an increase in the blockage ratio should lead to an increase in St. [3] Furthermore, Okajima (1982) found in his experimental investigation on rectangular cylinders under free stream conditions a local maximum of the Strouhal number at the same Reynolds number as Franke et al. (1990) and the present study. In conclusion, the St data for confined square cylinder flow taken from the literature are highly scattered. The corresponding values for free stream conditions at least show a local maximum at the same Reynolds number as in the present work, but the values cannot be compared directly owing to the influence of blockage. However, in view of these large deviations, the differences between the computed LBA and FVM results are only marginal.

4.3.3. Drag and lift coefficients

In the unsteady 2D flow regime ($60 \leqslant Re \leqslant 300$) the near-wake becomes unstable and a sinusoidal oscillation of the shear layers commences, later forming the von Kármán vortex street. In Fig 10(a), the time-averaged drag coefficients in this Re range are plotted for the three FVM computations. The $C_d(Re)$ curve has a local minimum at $Re \approx 150$. Up to

$Re \approx 100$ to 150 good agreement is achieved on the three different grids. However, for larger Re the C_d values on the coarsest grid deviate strongly from the data on the two finer grids, which are in close agreement. This discrepancy is clearly caused by the insufficient resolution of the cylinder vicinity for the coarse grid, which plays a dominant role especially in the Re range at which separation moves from the trailing to the leading edge of the cylinder. Fig 10(b) shows a comparison of the LBA and FVM results both obtained on the finest grid level. The agreement between the LBA and FVM data is satisfactory up to $Re \approx 100$. Above this value, the drag coefficients computed by LBA are systematically higher. Comparison of Fig. 10(a) and (b) shows that the LBA data on the finest grid are in close agreement with the FVM on the coarsest grid. Therefore, the deviations between LBA and FVM results on the finest grids are expected again to be an effect of insufficient resolution for LBA, especially in the vicinity of the cylinder.

No experimental or other numerical data for comparison were found in the literature for the same inflow conditions and blockage ratio. However, at least the computations of Franke (1991) and Franke et al. (1990) for a square cylinder under free stream conditions confirm our finding of a local C_d minimum approximately at the Reynolds number where separation is initiated at the leading edge.

Finally, in Fig. 11 the variation of the drag coefficient $(\max(C_d) - \min(C_d))$ and the lift coefficient $(\max(C_l) - \min(C_l))$ are plotted for the FVM computations. The amplitudes of the C_l oscillations are about one order of magnitude larger than the corresponding drag values. The drag variation

---

[3] Note that in the present study Re and St are based on the maximum flow velocity of the parabolic inflow profile and that a redefinition based on the mean velocity would change the comparison with the free stream case.

increases progressively over the entire *Re* range, whereas for the lift variation a degressive increase is observed up to $Re \approx 150$ followed by an inflexion point. The results on the two finer grids are in close agreement. Only on the coarse grid no reasonable results are obtained above the inflexion point owing to the resolution problem already discussed. No data were found in the literature for the variation of drag and lift of confined square cylinders. Only the work of Franke (1991) reports a similar curve for the amplitude of the lift coefficient, but for free stream conditions which make a direct comparison impossible.

5. Conclusions

A lack of accurate and detailed data was found in the literature for the confined laminar flow past a square cylinder, which initiated the present work. In order to generate reliable numerical results, two totally different approaches were applied to investigate the 2D flow past a square cylinder inside a channel $(B = 1/8)$ for the Reynolds number range $0.5 \leqslant Re \leqslant 300$. For both methods, a lattice-Boltzmann automata developed for equidistant orthogonal lattices and a general-purpose FVM, grid independence of the results was investigated first. For steady flow $(Re < 60)$ excellent agreement between the LBA and FVM results was found for the length of the recirculation region. Small deviations were detected for the drag coefficients in the lower *Re* range. The unsteady flow computations impressively demonstrate the capability of the LBA to deal with instantaneous flows. Velocity profiles at different locations in the flow field $(Re = 100)$ were evaluated and compared with the FVM data, showing very good agreement. Strouhal numbers were determined for the entire Reynolds number range. Both methods provide a local maximum of *St* at $Re \approx 150$. Compared with the scattered data in the literature, the deviations between the LBA and FVM results are almost negligible. Finally, drag coefficients were computed and compared. As is known from the literature for square cylinders in free stream, the drag coefficient of a confined cylinder also shows a local minimum at $Re \approx 150$. In conclusion, the present work provides reliable and accurate results for the confined cylinder flow which were not available before. The extension to 3D computations and higher Reynolds numbers is the subject of further investigations within ongoing research.

References

Bernsdorf, J., Schäfer, M., 1997. Practical aspects of the simulation of viscous flow using lattice-Boltzmann automata. In: Helmig, R., Jäger, W., Kinzelback, W., Knabner, P., Wittum, G. (Eds.), Modeling and Computation in Environmental Sciences. Notes on Numerical Fluid Mechanics, vol. 59. pp. 61–71.

Bernsdorf, J., Zeiser, T., Brenner, G., Durst, F., 1998. Simulation of 2D channel flow around a square obstacle with lattice-Boltzmann (BGK) automata. In: Proceedings of the Seventh International Conference on the Discrete Simulation of Fluids. University of Oxford, 14–18 July 1998. Int. J. Modern Phys. C 9 (8), 1129–1141.

Bernsdorf, J., Durst, F., Schäfer, M., 1999. Comparison of cellular automata and finite-volume techniques for simulation of incompressible flows in complex geometries. Int. J. Numer. Meth. Fluids. 29, 251–264.

Bhatnagar, P., Gross, E.P., Krook, M.K., 1954. A model for collision processes in gases in small amplitude processes in charged and neutral one-component systems. Phys. Rev. 94, 511–525.

Breuer, M., Rodi, W., 1994. Large-eddy simulation of turbulent flow through a straight square duct and a 180° bend. In: Fluid Mechanics and its Applications, vol. 26. In: Voke, P.R., Kleiser, L., Hollet, J.P. (Eds.), Direct and Large-Eddy Simulation I. Selected Papers from the First ERCOFTAC Workshop on Direct and Large-Eddy Simulation. Guildford, Surrey, UK, 27–30 March 1994. Kluwer Academic Publishers, Dordrecht, pp. 273–285.

Breuer, M., Lakehal, D., Rodi, W., 1996. Flow around a surface mounted cubical obstacle: comparison of LES and RANS – Results. In: IMACS–COST Conference on Computational Fluid Dynamics. Three-dimensional Complex Flows, Lausanne, Switzerland, 13–15 Septmeber 1995. In: Deville, M., Gavrilakis, S., Rhyming, I.L. (Eds.), Computation of 3D Complex Flows. Notes on Numerical Fluid Mechanics, vol. 53. Vieweg Verlag, Braunschweig, pp. 22–30.

Breuer, M., Pourquié, M., 1996. First experiences with LES of flows past bluff bodies. In: Proceedings of the Third International Symposium of Engineering Turbulence Modelling and Measurements, Heraklion, Crete, Greece, 27–29 May 1996. In: Rodi, W., Bergeles, G. (Eds.), Engineering Turbulence Modelling and Experiments 3. Elsevier, Amsterdam, pp. 177–186.

Breuer, M., Rodi, W. 1996. Large-eddy simulation of complex turbulent flows of practical interest. In: Hirschel, E.H. (Ed.), Flow Simulation with High-Performance Computers II. Notes on Numerical Fluid Mechanics, vol. 52. Vieweg Verlag, Braunschweig, pp. 258–274.

Breuer, M., 1998a. Numerical and modeling influences on large eddy simulations for the flow past a circular cylinder. In: Proceedings of the 11th Symposium on Turbulent Shear Flows, vol. 3, Grenoble, France, 8–11 September 1997, pp. 26:7–26:12; Int. J. Heat Fluid Flow 19 (5), 512–521.

Breuer, M., 1998b. Large eddy simulation of the sub-critical flow past a circular cylinder: numerical and modeling aspects. Int. J. Numer. Meth. Fluids 28, 1281–1302.

Breuer, M., 1999. Large eddy simulation of high Reynolds number circular cylinder flow. In: Proceedings of the Workshop on Industrial and Environmental Applications of Direct and Large-Eddy Simulation, 5–7 August 1998. Boğaziçi University, Istanbul, Turkey. In: Biringen, S., Örs, H., Tezel, A., Ferziger, J.H. (Eds.), Lecture Notes in Physics, vol. 529. Springer, Berlin, pp. 176–189.

Davis, R.W., Moore, E.F., 1982. A numerical study of vortex shedding from rectangles. J. Fluid Mech. 116, 475–506.

Eggels, J.G.M., Somers, J.A., 1995. Numerical simulation of the free convective flow using the lattice-Boltzmann scheme. Int. J. Heat Fluid Flow 16, 357–364.

Eggels, J.G.M., 1996. Direct and large-eddy simulation of turbulent fluid flow using the lattice-Boltzmann scheme. Int. J. Heat Fluid Flow 17, 307–323.

Davis, R.W., Moore, E.F., Purtell, L.P., 1984. A numerical-experimental study of confined flow around rectangular cylinders. Phys. Fluids 27 (1), 46–59.

Franke, R., 1991. Numerische Berechnung der instationären Wirbelablösung hinter zylindrischen Körpern. Ph.D. Thesis. University of Karlsruhe.

Franke, R., Rodi, W., Schönung, B., 1990. Numerical calculation of laminar vortex shedding past cylinders. J. Wind Eng. Ind. Aerodyn. 35, 237–257.

Frisch, U., D'Humiéres, D., Hasslacher, B., Lallemand, P., Pomeau, Y., Rivert, J.P., 1987. Lattice-gas hydrodynamics in two and three dimensions. Complex Sys. 1, 649–707.

Inamuro, T., Yoshine, M., Ogino, F., 1995. A non-slip boundary condition for lattice-Boltzmann simulations. Phys. Fluids 7 (12), 2928–2930.

Klekar, K.M., Patankar, S.V., 1992. Numerical prediction of vortex shedding behind square cylinders. Int. J. Numer. Meth. Fluids 14, 327–341.

Kobayashi, M.H., Pereira, J.C.F., 1991. Numerical comparison of momentum interpolation methods and pressure–velocity algorithms using non-staggered grids. Commun. Appl. Numer. Meth. 7, 173–186.

Li, G., Humphrey, J.A.C., 1995. Numerical modelling of confined flow past a cylinder of square cross-section at various orientations. J. Numer. Meth. Fluids 20, 1215–1236.

Maier, R.S., Bernard, R.S., 1997. Accuracy of the lattice-Boltzmann method. In: Proceedings of the Sixth International Conference on the Discrete Models for Fluid Mechanics. Boston University, Boston, 26–28 August 1996. Int. J. Modern Phys. C 8 (4), 747–752.

Miller, T.F., Schmidt, F.W., 1988. Use of pressure-weighted interpolation method for the solution of the incompressible Navier–Stokes equations on a non-staggered grid system. Numer. Heat Transfer 14, 213–233.

Mukhopadhyay, A., Biswas, G., Sundararajan, T., 1992. Numerical investigation of confined wakes behind a square cylinder in a channel. Int. J. Numer. Meth. Fluids 14, 1473–1484.

Noble, D.R., Georgiadis, J.G., Buckius, R.O., 1995a. Direct assessment of lattice-Boltzmann hydrodynamics and boundary conditions for recirculation flows. J. Stat. Phys. 81 (1/2), 17–33.

Noble, D.R., Chen, S., Georgiadis, J.G., Buckius, R.O., 1995b. A consistent hydrodynamic boundary condition for the lattice-Boltzmann method. Phys. Fluids 7, 203–209.

Okajima, A., 1982. Strouhal numbers of rectangular cylinders. J. Fluid Mech. 123, 379–398.

Okajima, A., 1990. Numerical simulation of flow around rectangular cylinders. J. Wind Eng. Ind. Aerodyn. 33, 171–180.

Qian, Y.H., D'Humiéres, D., Lallemand, P., 1992. Lattice-BGK models for Navier–Stokes equation. Europhys. Lett. 17 (6), 479–484.

Rhie, C.M., Chow, W.L., 1983. A numerical study of the turbulent flow past an isolated airfoil with trailing edge separation. AIAA J. 21, 1225–1532.

Shair, F.H., Grove, A.S., Petersen, E.E., Acrivos, A., 1963. The effect of confining walls on the stability of the steady wake behind a circular cylinder. J. Fluid Mech. 17, 546–550.

Skordos, P.A., 1993. Initial and boundary conditions for the lattice-Boltzmann method. Phys. Rev. E 48, 4823–4842.

Suzuki, H., Inoue, Y., Nishimura, T., Fukutani, F., Suzuki, K., 1993. Unsteady flow in a channel obstructed by a square rod (crisscross motion of vortex). Int. J. Heat Fluid Flow 14 (1), 2–9.

Williamson, C.H.K., 1996. Vortex dynamics in the cylinder wake. Annu. Rev. Fluid Mech. 28, 477–539.

Zdravkovich, M.M., 1997. Flow Around Circular Cylinders, vol. 1: Fundamentals. Oxford University Press, New York.

Zeiser, T., 1998. Numerische Simulation der instationären Umströmung eines quadratischen Zylinders mit einem Lattice-Boltzmann Verfahren, Thesis. Institute of Fluid Mechanics, University of Erlangen–Nürnberg.

Ziegler, D.P., 1993. Boundary conditions for lattice-Boltzmann simulations. J. Stat. Phys. 71, 1171–1177.